Seismic tuning of dispersive thin layers

Seismic Tuning of Dispersive Thin Layers

Giorgos Papageorgiou*[1, 2] and Mark Chapman [1]

[1] School of Geosciences, Grant Institute, West Mains Road, Edinburgh, EH9 3JW, UK
[2] Department of Geoscience,, NTNU S.P. Andersensvei 15A,, 7491 Trondheim, Norway

July 13, 2020

Abstract

The wedge model is commonly used to study the limits of seismic resolution where conventionally the thickness of sub-resolution seismic layers can be determined from thin layer tuning curves. Tuning curves relate the layer temporal thickness to the wavelet frequency but, to our knowledge, no systematic study has been done to date of the effects of velocity dispersion and attenuation on tuning. In this work we study the tuning properties of a thin layer dispersing according to the standard linear solid model. We show that the first tuning curve is sensitive to the attenuation, relative polarity and magnitude of the two reflection coefficients at the top and base of the layer. We provide an analytic formula for the upper bound in the mismatch between the elastic and dispersive tuning curves. We conclude that highly attenuative thin layers can appear thicker or thinner than they actually are depending on polarity and relative magnitude of reflection coefficients at the layer interfaces. Our results are particularly relevant in the quantification of CO_2 where knowledge of the temporal thickness of CO_2 layers is reliant on their tuning curves.

*giorgos.papageorgiou@ed.ac.uk

1 Introduction

One of the goals of seismic interpretation is to relate seismic amplitude variations to rock and fluid properties from variations in acoustic impedance. However, when geological layers are thinner than the seismic wavelength, interference form their top and base distorts the relation between seismic amplitude and acoustic impedance. Starting from the systematic approach of Widess (1973), much research has been done in the past to understand this interference by studying the tuning properties of waves encountering thin layers.

Notably properties of thin layer tuning are used in carbon monitoring for the quantification of CO_2 injected in depleted reservoirs using spectral characteristics (Williams & Chadwick, 2012; Huang et al., 2016; White et al., 2018; Ivandic et al., 2018) or time delays (Arts et al., 2004; Furre et al., 2015). These are based on earlier modelling works (De Voogd & Den Rooijen, 1983; Chung & Lawton, 1995b,a) all of which assume thin layers to be elastic and the reflection coefficients real-valued.

There is increasing evidence however that a range of dispersion mechanisms affect seismic wave propagation all of which are relevant in carbon monitoring. For example, patchy fluid saturation as well as wave induced flow from large-scale fractures (see Müller et al., 2010; Caspari et al., 2011; Germán Rubino & Velis, 2011; Papageorgiou & Chapman, 2017; Falcon-Suarez et al., 2018) have been shown to affect seismic wave propagation. But the tuning properties of such dispersive thin layers have not been investigated.

In this paper we revisit the wedge model and use it to understand tuning properties of dispersive thin layers. We assume a thin layer that disperses according to the standard linear solid (SLS) model (Ursin & Toverud, 2002), and calculate the shift induced by attenuation in its tuning curves as well as the upper bound in this shift. It should be noted, that we do not consider different dissipation mechanisms i.e. due to solid-solid friction or contact-line movement (Rozhko, 2020; Winkler & Nur, 1982) in which dispersion depends on wave amplitude rather than frequency, but postpone such considerations for future work. Likewise, the wedge model we discuss here is assumed homoegeneous although this is not always the case, particularly in the context of CO_2 monitoring (Glubokovskikh et al., 2020).

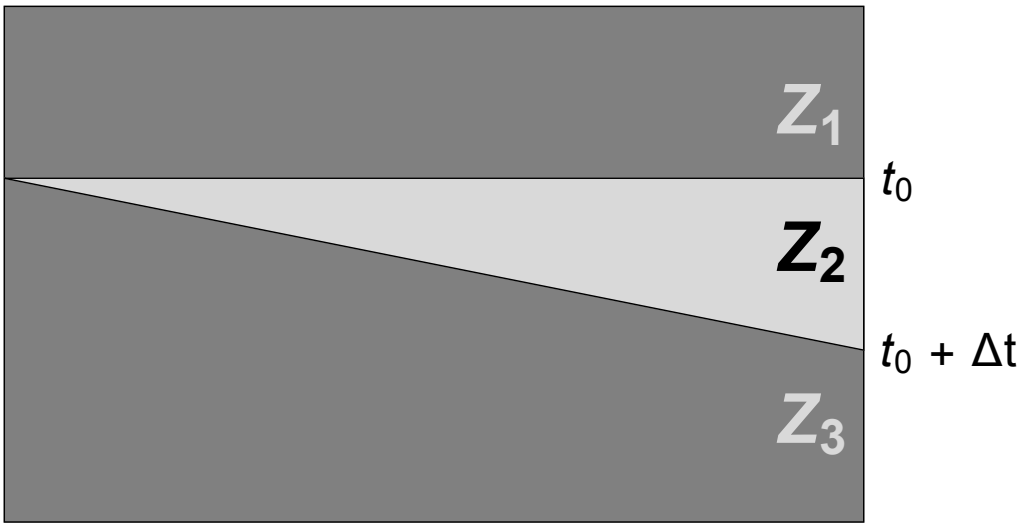

Figure 1: A wedge model of linearly increasing temporal thickness and acoustic impedance Z_2 is encased within two half-spaces of acoustic impedance Z_1, Z_3 respectively. Varying amplitude, apparent temporal thickness and spectral characteristics of such a configuration help in the study of seismic resolution limits and tuning.

2 Elastic Layer Tuning

Let us consider the properties of the wedge model depicted in Fig. 1 and its normal incidence reflection coefficient time series given by

$$R_E(t) = r_1\ \delta(t - t_0)\ +\ r_2\ \delta(t - t_0 - \Delta t), \tag{1}$$

or, in the frequency domain:

$$R_E(\omega) = r_1\ e^{-\mathrm{i}\omega t_0}\ +\ r_2\ e^{-\mathrm{i}\omega(t_0+\Delta t)}, \tag{2}$$

where the normal incidence reflection coefficients are given by the impedance contrast between consecutive layers:

$$r_i = \frac{Z_{i+1} - Z_i}{Z_{i+1} + Z_i}, \qquad i = 1, 2, \tag{3}$$

and index E indicates elastic modelling. The wedge model of Fig. 1 is use-

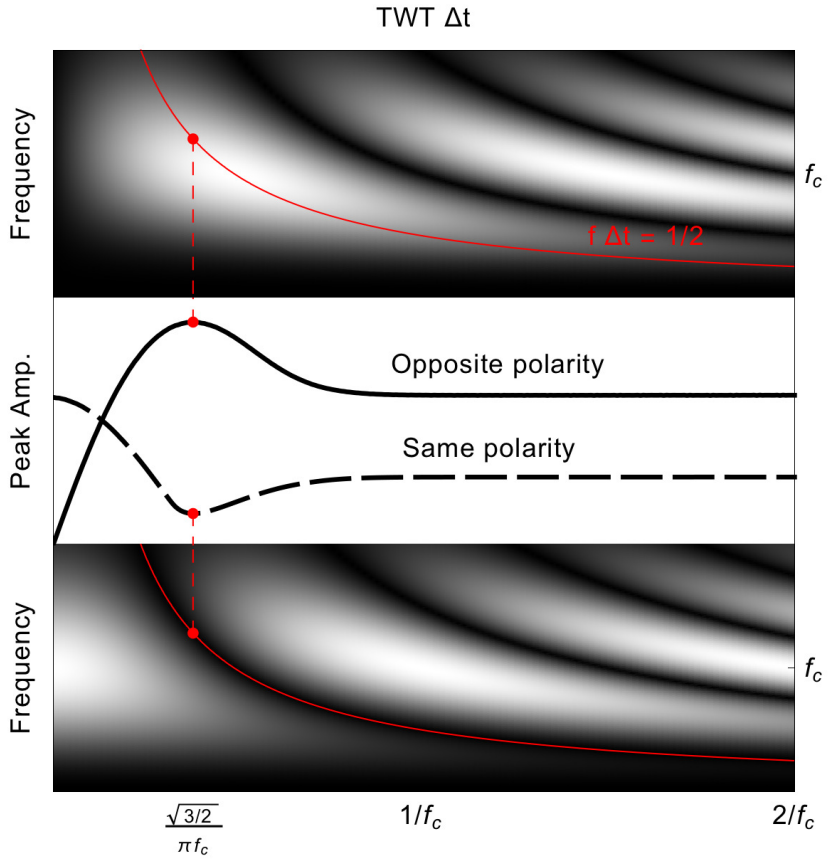

Figure 2: Spectral and amplitude characteristics of a zero phase ricker wavelet encountering an elastic wedge. The tuning thickness, marked with a red dashed line, is explicitly denoted as a function of wavelet central frequency f_c for top/base reflections of opposite and same polarity.

ful for studying tuning which occurs when interference from top and base of layer 2 is maximum. Based on Eq. (2), the amplitude spectrum takes extreme value (minimum/maximum for opposite/same polarity reflections respectively) when $f\Delta t = n/2, \quad n = 1, 2, \dots$. The first of these, i.e.

$$f\Delta t = \frac{1}{2} \tag{4}$$

defines the 1st tuning curve of the thin bed (Chung & Lawton, 1995b) and it has been used in seismic imaging to resolve layer thickness. For example, a zero phase Ricker wavelet with spectrum $W(\omega)$ and central angular frequency $\omega_c = 2\pi f_c$ defined by (see Wang, 2015)

$$W(\omega) = \frac{2\omega^2}{\sqrt{\pi}\omega_c^3} e^{-\left(\frac{\omega}{\omega_c}\right)^2}, \tag{5}$$

will have an effective frequency corresponding to the wavelength between its two troughs $f_{\text{eff.}} = \frac{\pi}{\sqrt{6}}\, f_c$ and tune at temporal thickness $\Delta t = \frac{\sqrt{3/2}}{\pi f_c}$ according to (4). The spectral and amplitude characteristics of such a configuration are shown in Fig. 2 with the tuning thickness $\frac{\sqrt{3/2}}{\pi f_c}$ clearly marked to show the maximum (rep. minimum) amplitude as well as the first tuning curve. It is clear that for the reflectivity time series in Eq. (2) these characteristics depend solely on relative polarity between top and base of the layer.

3 Dispersive Layer tuning

For the remainder of this paper we investigate how spectral and amplitude characteristics are affected when layer 2 of Fig. 1 is dispersive, where dispersion implies that layer 2 has a complex-valued, frequency-dependent acoustic impedance $\widetilde{Z}_2$ given by:

$$\widetilde{Z}_2(\omega) = \rho\; c(\omega) \tag{6}$$

where ρ the density of the medium and the frequency dependence is dictated by its phase velocity $c(\omega)$. Likewise, the normal incidence reflection coefficients $\tilde{r}_1, \tilde{r}_2$ become frequency dependent and complex valued. They are derived by matching stress and strain boundary conditions at each interface (see Innanen, 2011):

$$\tilde{r}_1(\omega) = \frac{\widetilde{Z}_2(\omega) - Z_1}{\widetilde{Z}_2(\omega) + Z_1}, \qquad \tilde{r}_2(\omega) = \frac{Z_3 - \widetilde{Z}_2(\omega)}{Z_3 + \widetilde{Z}_2(\omega)}. \tag{7}$$

With $\tilde{r}_1, \tilde{r}_2$ we obtain the modified reflectivity series:

$$R_D(\omega) = \tilde{r}_1(\omega)\ e^{-\mathrm{i}\omega t_0}\ +\ \tilde{r}_2(\omega)\ e^{-\mathrm{i}\omega(t_0+\Delta t)}, \tag{8}$$

where we use index D to indicate dispersive modelling.

It is clear that Eq. (7) and (8) depend on the choice of the velocity model $c(\omega)$ of Eq. (6) which we choose to be a standard linear solid (SLS) (e.g. Ursin & Toverud, 2002) whose impedance $\widetilde{Z}_2(\omega)$ is the product of the elastic impedance Z_2 and a complex function

$$\widetilde{Z}_2(\omega;\alpha,\tau) = Z_2\ \sqrt{\frac{1+\mathrm{i}\alpha\omega\tau}{1+\mathrm{i}\omega\tau}}, \quad \alpha \geq 1 \tag{9}$$

where τ is a characteristic time scale and α is the ratio of unrelaxed to relaxed wave moduli (see Fig. 3). It is straightforward to see that

$$\lim_{\omega\to 0} \widetilde{Z}_2(\omega;\alpha,\tau) = \lim_{\alpha\to 1} \widetilde{Z}_2(\omega;\alpha,\tau) = Z_2. \tag{10}$$

These limits are useful if the time scale of the observation can be assumed small relative to the time scale of the model i.e. if the impedance Z_2 is observed at reference frequency $\omega_0 = 0$ and its behaviour is extrapolated to non-zero frequency by means of the SLS. Alternatively one may choose reference frequency $\omega_0 = 1/\tau$ where attenuation peaks to:

$$\frac{1}{Q_{\min}} = \frac{\alpha-1}{2\sqrt{\alpha}}, \tag{11}$$

and define some reference, zero-frequency real-valued acoustic impedance Z_0 such that:

$$\frac{Z_2}{Z_0} = \mathrm{Re}\left(\tilde{Z}_2(1/\tau;\alpha,\tau)\right) \simeq \frac{3+\alpha}{4} + \mathcal{O}((\alpha-1)^2), \tag{12}$$

which is used to extrapolate the impedance when $\omega \neq \omega_0$.

In practical terms, the former choice $\omega_0 = 0$, involves contribution of both amplitude and phase from the SLS whereas the latter choice $\omega_0 = 1/\tau$ of only phase. Here we chose the latter to isolate the potentially neglected effect of phase shift at the wedge interfaces. Using Eq. (12) and using only first orders in $\alpha - 1$, the reflection coefficients become:

$$\begin{aligned}
\tilde{r}_1'(\omega) &\simeq r_1 + \frac{1-\omega^2\tau^2-2\mathrm{i}\omega\tau}{8(1+\omega^2\tau^2)}\left(r_1^2-1\right)(\alpha-1) \\
\tilde{r}_2'(\omega) &\simeq r_2 - \frac{1-\omega^2\tau^2-2\mathrm{i}\omega\tau}{8(1+\omega^2\tau^2)}\left(r_2^2-1\right)(\alpha-1),
\end{aligned} \tag{13}$$

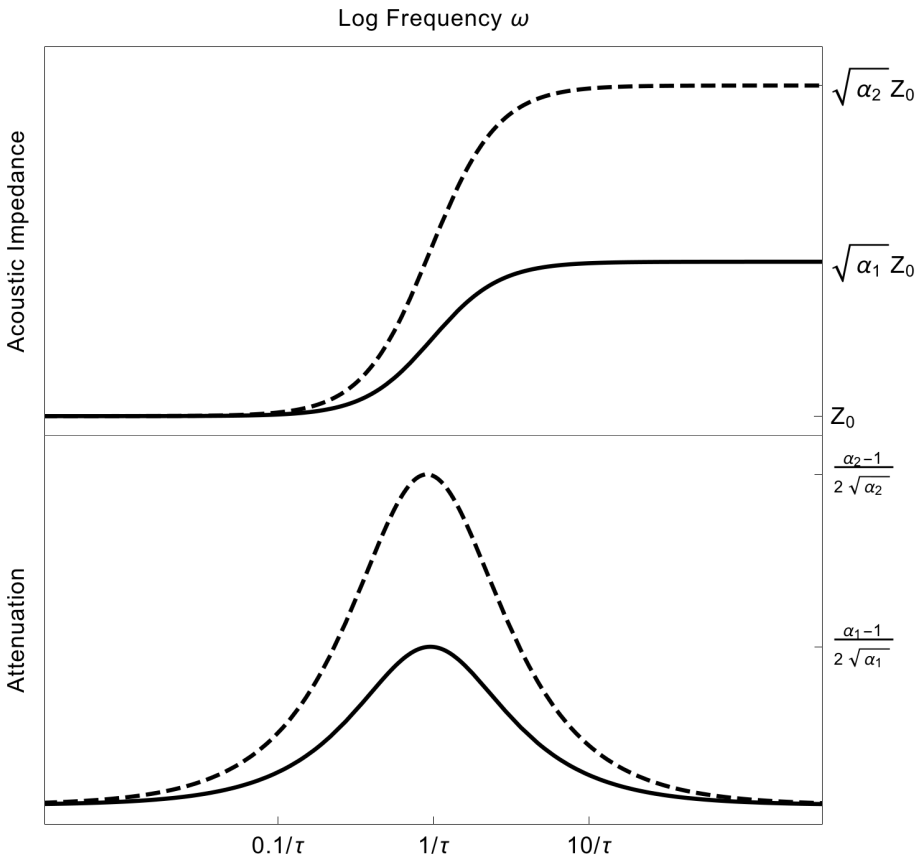

Figure 3: Shape of viscoelastic impedance $Z(\omega)$ and attenuation $1/Q$ derived from the Standard Linear Solid model. Different values of the parameter α lead to different attenuation curves. The model has a complex phase that is significant within a bandwidth of roughly two orders of magnitude around the relaxation frequency $1/\tau$.

and at $\omega_0 = 1/\tau$:

$$\begin{aligned} \tilde{r}_1'(\omega_0) &\simeq r_1 + \frac{\mathrm{i}}{8}\left(1 - r_1^2\right)(\alpha - 1) \\ \tilde{r}_2'(\omega_0) &\simeq r_2 - \frac{\mathrm{i}}{8}\left(1 - r_2^2\right)(\alpha - 1)\,. \end{aligned} \tag{14}$$

Inserting the reflection coefficients of Eq. (13) in the dispersive reflectivity series in Eq. (8) we find that the first tuning curve at the extreme of $|R_D(\omega)|$ has the form:

$$f\Delta t = \frac{1}{2} + \phi(\omega, \alpha, r_1, r_2) \tag{15}$$

where ϕ takes the following simple form at $\omega = \omega_0$

$$\phi(\omega_0, \alpha, r_1, r_2) = \frac{(r_1 + r_2)(1 - r_1 r_2)(1 - \alpha)}{16\pi\ r_1 r_2}. \tag{16}$$

A reasonable upper bound for ϕ of Eq. (16), is obtained if we constrain the attenuation to $1/Q_{\min} \leq 0.1$, ($1 \leq \alpha \lesssim 1.22$) which still retains a good approximation in using the first order expansion in $\alpha - 1$.

In Fig. 4 we show the quantity ϕ against the magnitude of the reflection coefficients at the top (r_1) and base (r_2) of the wedge for $Q = 10$ when $\omega_0 = 1/\tau$. It is apparent from Fig. 4, that the tuning of the viscoelastic wedge depends nontrivially on the relative magnitude of reflection coefficient pairs. We choose eight representative reflection coefficient pairs marked in Fig. 4 based on the classification of Chung & Lawton (1995b) (see also Puryear & Castagna, 2008) where reflectivity pairs belong in one of four types (all permutations of equal/unequal magnitude and same/opposite polarity).

Additionally we also distinguish between positive/negative polarity of the first reflection which determines whether the wavelet acquires phase retardation or advancement at the dispersive interface. It is evident from Fig. 4 that cases where the top reflection is smaller (in absolute terms) than the base reflection do not need separate consideration due to the symmetry.

Together with their respective Chung & Lawton (1995b) types the following reflectivity pairs are marked on Fig. 4:

- Type I: Opposite polarity-equal magnitude (white square/circle) with $r_1 = \mp 0.15,\ r_2 = \pm 0.15$ respectively
- Type II: Equal polarity-equal magnitude (white cross/triangle) with $r_1 = \mp 0.15,\ r_2 = \mp 0.15$ respectively

r_1 Polarity	Type I	Type II	Type III	Type IV
+ve	No Error	-6%	12%	-17%
$-$ve	No Error	6%	-12%	17%

Table 1: A table indicating maximum errors (for $Q \simeq 10$) that can be made in thickness estimation of thin beds when ignoring the impact of viscoelastic effects in tuning. The error depends on the type of top-bottom reflectivity magnitude as well as relative polarity.

- Type III: Opposite polarity-unequal magnitude (black square/circle) with $r_1 = \mp 0.15,\ r_2 = \pm 0.03$ respectively
- Type IV: Equal polarity-unequal magnitude (black cross/triangle) with $r_1 = \mp 0.15,\ r_2 = \mp 0.03$ respectively

Explicitly the tuning curves from the viscoelastic reflectivity series, as well as their amplitude characteristics from convolution with a zero-phase Ricker wavelet of Eq. (5) are shown in Fig. 5 together with the corresponding elastic models for comparison. Apart from Type I, the rest of the reflectivity types show measurable difference illustrating the potential for mis-estimation of layer thickness if viscoelasticity is neglected. We have calculated this error in Table 1 which represent what we consider to be an upper bound, rather than typical values. This is reflected on our choice of low quality factor ($Q \simeq 10$) as well as the ratio $5:1$ of top-base reflectivity for pairs of type III and IV; higher ratio of reflectivity pairs would yield the smallest of them very difficult to observe.

4 Discussion

We found that when intra-layer multiples are taken into account, the form for ϕ in Eq. (15) is similar both in form and in magnitude to Fig. 4 but we could not find a simple analytic expression like Eq. (16) in this case. Our work implies that highly attenuative thin layers introduce negligible energy loss but significant phase shifts. Therefore, in order to improve layer thickness estimates, we need a measurement independent of seismic amplitude like a well log, or an estimate of the attenuation in the layer which further implies that confident knowledge of one of thickness or attenuation (and the reflection

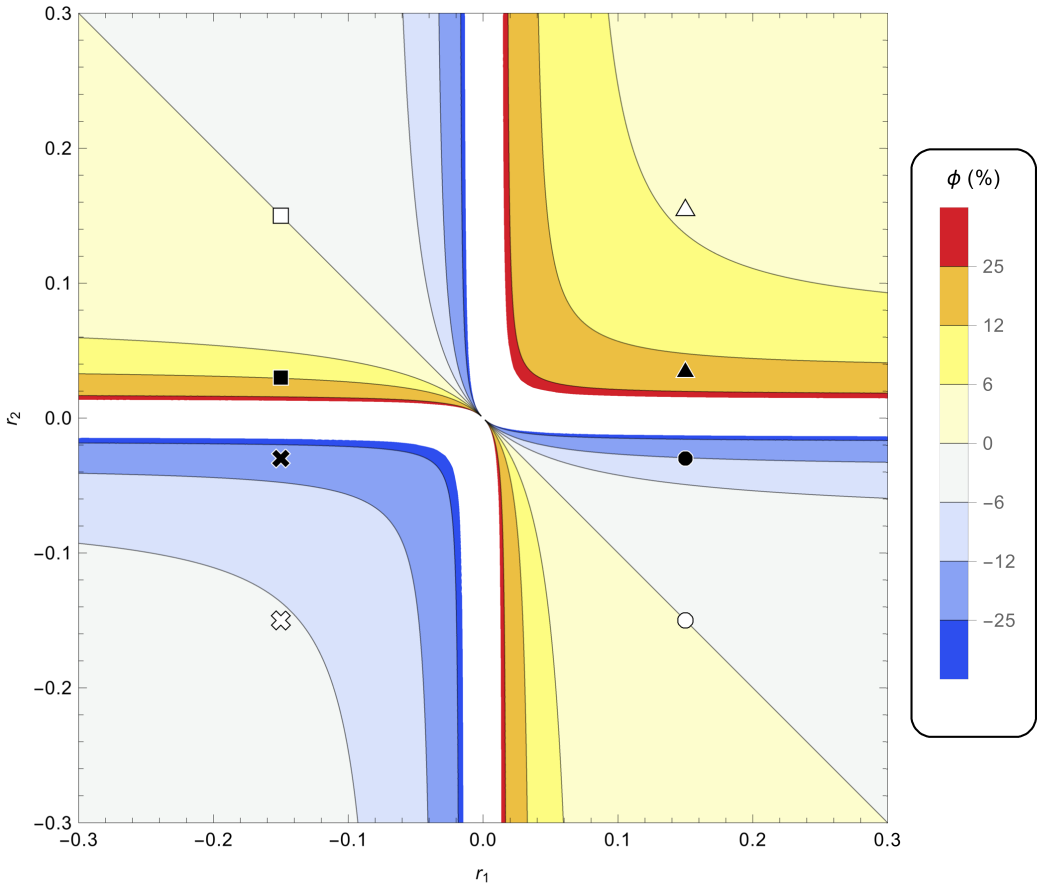

Figure 4: Difference of dispersive tuning curves from their elastic counterparts as quantified by the quantity ϕ from Eq. (16) for the upper bound $Q \simeq 10$ at reference frequency $\omega_0 = 1/\tau$. Eight reflection coefficient pairs are marked to represent different types of reflectivity as per Chung & Lawton (1995a) but also distinguishing between positive/negative first reflection as detailed in page 8.

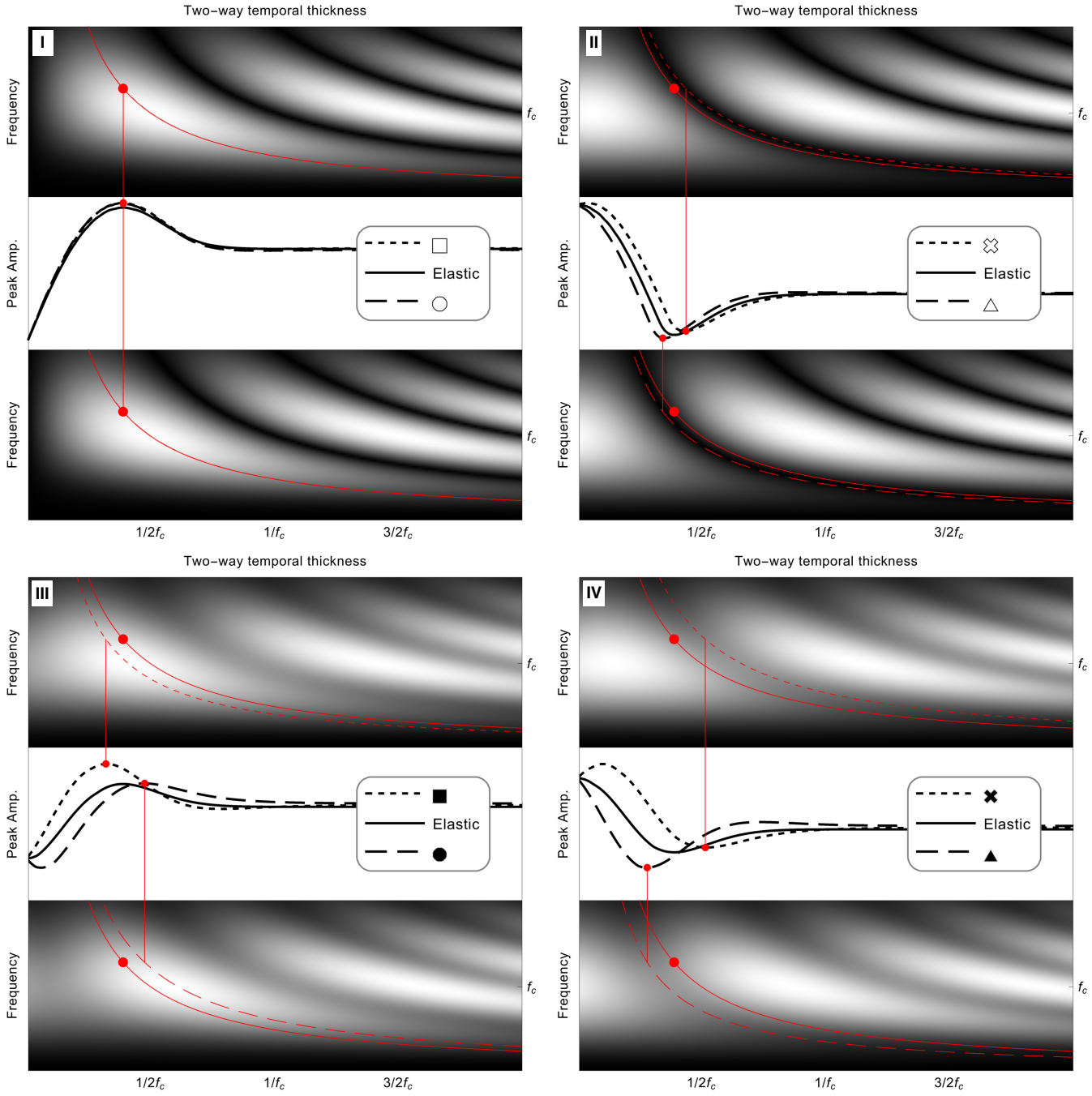

Figure 5: Comparison between peak wavelet amplitudes of elastic and viscoelastic wedges is shown in the middle panel of figures I-IV. The labelling of the figures follows the top/base reflectivity classification of Chung & Lawton (1995b). Spectral amplitude together with the shifted tuning curves for the viscoelastic wedge are shown above (when the first reflection is negative) and below (when the first reflection is positive) the amplitude plots in each figure, with a red point marking the elastic tuning thickness for the effective wavelet frequency. The filled/hollow square, cross, circle and triangle symbols refer to reflectivity pairs marked in Fig. 4.

coefficients at the top and base layer) can be used to invert for the other via Eq. (16).

5 Conclusions

We demonstrated that tuning of dispersive layers depends on attenuation as well as the polarity and magnitude of the reflection coefficients at the top and base of the layer. We showed that traditional tuning analysis of highly dispersive thin layers ($Q \simeq 10$) can lead to more than 10% mis-estimation in layer thickness if dispersion is ignored. The potential for mis-estimation is larger if the reflection coefficients from top and base layer have different magnitude.

Data Availability Statement

Data sharing is not applicable to this article as no new data were created or analyzed in this study.

Acknowledgments

We acknowledge financial support from the Research Council of Norway (RCN grant number: 267765). We also thank Alexey Stovas and Stanislav Glubokovskikh for their constructive comments on drafts of this work, as well as Alexander Rozhko and an anonymous reviewer for their reviews. GP acknowledges financial support from the UK CCSRC (funded by the EPSRC as part of the RCUK Energy Programme) for an IRC spent at Curtin University. He is grateful for the hospitality of Boris Gurevich and Stanislav Glubokovskikh and the creative and stimulating environment they contributed to.

Figure Legend list:

Figure 4: legend contains 8 percentage bands

References

Arts, R., Eiken, O., Chadwick, A., Zweigel, P., Van der Meer, L., & Zinszner, B., 2004. Monitoring of co_2 injected at sleipner using time-lapse seismic data, *Energy*, **29**(9), 1383–1392.

Caspari, E., Müller, T., & Gurevich, B., 2011. Time-lapse sonic logs reveal patchy co2 saturation in-situ, *Geophysical Research Letters*, **38**(13).

Chung, H. & Lawton, D., 1995a. Frequency characteristics of seismic reflections from thin beds, *Canadian Journal of Exploration Geophysicists*, **31**(1), 32–37.

Chung, H.-M. & Lawton, D. C., 1995b. Amplitude responses of thin beds: Sinusoidal approximation versus ricker approximation, *Geophysics*, **60**(1), 223–230.

De Voogd, N. & Den Rooijen, H., 1983. Thin-layer response and spectral bandwidth, *Geophysics*, **48**(1), 12–18.

Falcon-Suarez, I., Papageorgiou, G., Chadwick, A., North, L., Best, A. I., & Chapman, M., 2018. Co2-brine flow-through on an utsira sand core sample: Experimental and modelling. implications for the sleipner storage field, *International journal of greenhouse gas control*, **68**, 236–246.

Furre, A.-K., Kiær, A., & Eiken, O., 2015. Co2-induced seismic time shifts at sleipner, *Interpretation*, **3**(3), SS23–SS35.

Germán Rubino, J. & Velis, D. R., 2011. Seismic characterization of thin beds containing patchy carbon dioxide-brine distributions: A study based on numerical simulations, *Geophysics*, **76**(3), R57–R67.

Glubokovskikh, S., Pevzner, R., Gunning, J., Dance, T., Shulakova, V., Popik, D., Popik, S., Bagheri, M., & Gurevich, B., 2020. How well can time-lapse seismic characterize a small co2 leakage into a saline aquifer: Co2crc otway 2c experiment (victoria, australia), *International Journal of Greenhouse Gas Control*, **92**, 102854.

Huang, F., Juhlin, C., Han, L., Kempka, T., Lüth, S., & Zhang, F., 2016. Quantitative evaluation of thin-layer thickness and co2 mass utilizing seismic complex decomposition at the ketzin co2 storage site, germany, *Geophysical Journal International*, **207**(1), 160–173.

Innanen, K. A., 2011. Inversion of the seismic AVF/AVA signatures of highly attenuative targets, *Geophysics*, **76**(1), R1–R14.

Ivandic, M., Bergmann, P., Kummerow, J., Huang, F., Juhlin, C., & Lueth, S., 2018. Monitoring co2 saturation using time-lapse amplitude versus offset analysis of 3d seismic data from the ketzin co2 storage pilot site, germany, *Geophysical Prospecting*, **66**(8), 1568–1585.

Müller, T. M., Gurevich, B., & Lebedev, M., 2010. Seismic wave attenuation and dispersion resulting from wave-induced flow in porous rocks—a review, *Geophysics*, **75**(5), 75A147–75A164.

Papageorgiou, G. & Chapman, M., 2017. Wave-propagation in rocks saturated by two immiscible fluids, *Geophysical Journal International*, **209**(3), 1761.

Puryear, C. I. & Castagna, J. P., 2008. Layer-thickness determination and stratigraphic interpretation using spectral inversion: Theory and application, *Geophysics*, **73**(2), R37–R48.

Rozhko, A. Y., 2020. Effective fluid bulk modulus in the partially saturated rock and the amplitude dispersion effects, *Journal of Geophysical Research: Solid Earth*, **125**(3), e2019JB018693.

Ursin, B. & Toverud, T., 2002. Comparison of seismic dispersion and attenuation models, *Studia geophysica et geodaetica*, **46**(2), 293–320.

Wang, Y., 2015. Frequencies of the ricker wavelet, *Geophysics*, **80**(2), A31–A37.

White, J. C., Williams, G., Chadwick, A., Furre, A.-K., & Kiær, A., 2018. Sleipner: The ongoing challenge to determine the thickness of a thin co 2 layer, *International Journal of Greenhouse Gas Control*, **69**, 81–95.

Widess, M., 1973. How thin is a thin bed?, *Geophysics*, **38**(6), 1176–1180.

Williams, G. & Chadwick, A., 2012. Quantitative seismic analysis of a thin layer of co 2 in the sleipner injection plume, *Geophysics*, **77**(6), R245–R256.

Winkler, K. W. & Nur, A., 1982. Seismic attenuation: Effects of pore fluids and frictional-sliding, *Geophysics*, **47**(1), 1–15.